Thermal Performance of a Novel Helically Coiled Oscillating Heat Pipe (HCOHP) for Isothermal Adsorption. An Experimental Study

Yeboah S. K.

Department of Architecture and Built Environment

Faculty of Science and Engineering

The University of Nottingham Ningbo China

199 Taikang East Road, Ningbo 315100, PR China

Email: Siegfried.yeboah@nottingham.edu.cn

Darkwa, J.

Department of Architecture and Built Environment

The University of Nottingham

University Park, Nottingham, NG7 2RD, UK

Email: J.Darkwa@nottingham.ac.uk

Abstract

Helically Coiled Oscillating Heat Pipes (HCOHPs) have been designed and tested under laboratory conditions to investigate their potential to achieve isothermal adsorption when integrated with a cylindrical solid desiccant packed bed system. The HCOHPs fabricated out of copper, are essentially single turn closed loop oscillating heat pipes with their evaporator and condenser sections helically coiled. They were charged with ethanol, methanol and deionised water respectively at approximately 60% volume fill ratio and tested by slotting through their helically coiled evaporators an empty cylindrical copper vessel which allowed hot air to be blown through at various heat loads to ascertain their thermal performances.

The results showed there were critical heat fluxes which varied with heat input amount at the evaporator, beyond which dry-out commenced and thermal resistance increased. These heat fluxes were $\leq 70W$ for the ethanol HCOHP and $\leq 105W$ for both the methanol and deionised water HCOHPs. Performance instabilities owing to liquid phase of the working fluid transitioning in the drying-out stage was observed for the methanol HCOHP beyond 234W. The variation of the effective thermal conductivities at the evaporators were found to influence the thermal contact resistance experienced at the contact interface of integration and the maximum heat input amount at the evaporators. Optimum performance between the HCOHPs was observed with the deionised water type. Overall, the HCOHPs were capable of managing relatively large amounts of heat input due to their helically coiled sections creating comparatively larger evaporator sections holding relatively more working fluid than the conventional serpentine single turn closed loop OHP system of the same volume and fill ratio. Investigations involving the visualization of the internal flow dynamics is recommended for future studies.

Keywords: Oscillating Heat Pipes (OHP), Heat Transfer, Working Fluids, Isothermalization, Thermal Resistance, Thermal Contact Resistance, Dry-Out

1. Introduction

Oscillating/pulsating heat pipes (OHPs/PHPs) developed by Akachi[1] in the early 1990s offer enhanced passive heat transfer using the oscillating movement of the working fluid and phase change phenomena[2-4]. As heat is added to their evaporator, the liquid phase of the working fluid vaporises, causing vapour volume expansion whilst in the condenser the vapour condenses into liquid, causing volume contraction. The volume expansion and contraction excite an oscillation motion of the liquid plugs and vapour bubbles in their wickless miniature channels. Through forced convection and phase-change, heat is transported from the evaporator to the condenser[5-6]. Continuous heating sustains the oscillation flow hence fluid transported from the evaporator section to the condenser section transfers heat from the higher temperature zone to the lower temperature zone[7].

For conventional heat pipes, limits on transport distance as a result of their wick structure along with associated configuration challenges in process applications influences their performance[8-11]. For instance, the basic structure of a closed loop PHP consists of a long capillary tube bent turn by turn and joined end to end, forming an elongated serpentine loop[12]. This typically long continuous wickless capillary tube structure bent into many turns and filled with working fluid makes their design and operating principle different from that of conventional heat pipes[13]. Tong et al[13] found that their meandering bends, uneven slug and plug distribution and non-concurrent boiling at the evaporator contributes to the driving and restoring forces for fluid circulation and oscillations.

Several OHPs have been designed to overcome spatial and configurational challenges, ones that typically may limit the application of conventional heat pipes in many processes. For instance, Qu et al[14] designed and fabricated a hybrid flexible oscillating heat pipe (FOHP) with its adiabatic section made of fluororubber tubes as potential thermal management solution for some spatially complicated energy utilization systems and found start-up and heat transfer characteristics partially degraded on bending the adiabatic section. Chien et al[15] carried out an experimental investigation on a closed loop PHP (CLPHP) with non-uniform channel configuration designed to introduce additional unbalancing capillary force aimed at resolving problems with fewer turn PHPs in horizontal orientation and found the non-uniform channel CLPHP functioned at all inclinations when the charge ratio was above 50%. Sriudom et al[16] developed a helical oscillating heat pipe (HOHP) to investigate its flow behaviours and complicated phenomena of flow patterns and heat transfer characteristics. Their design was such that the coils for the evaporator and condenser were in a series arrangement and returned through the coils again to form the adiabatic section. They studied the effect of evaporator temperature, pitch distance, and working fluid on the internal flow pattern and the heat transfer characteristics of their HOHP and observed 4 internal flow patterns, bubble flow, slug flow, annular flow, and stratified wavy flow, in the evaporator section for the working fluids used. They also observed the heat transfer rate decreasing with increased pitch distance. Yi et al[17]also carried out an experimental study on the heat transfer characteristics and the flow patterns of the evaporator section using small diameter coiled pipes in a looped heat pipe (LHP). For different filling ratios and heat fluxes they found that the combined effect of the evaporation of the thin liquid film, the disturbance caused by pulsation and the secondary flow enhanced greatly the heat transfer and the critical heat flux of the evaporator section. They also found that the slug flow is the main flow pattern in their smallest-coiled pipe with the pulsation having a remarkable influence on flow and heat transfer. Investigations by Liu et al[12] shows that the likelihood of circulatory flow in an OHP increases as it becomes less symmetric.

In this study, Helically Coiled Oscillating Heat Pipe (HCOHPs) devices have been designed and tested under laboratory conditions to investigate their potential to achieve isothermal adsorption on integrating with a cylindrical solid desiccant packed bed system oriented horizontally. The reason for this is that, in a packed bed of solid desiccants, the heat of adsorption raises the temperature of the bed and decreases the adsorption capacity, subsequently changing the exit process airstream humidity ratio and temperature[18-20]. Several studies including those carried out by Abd-Elrahman et al[21],

Ramzy et al[22], Hamed et al[23], Schindler and LeVan[24], Liu and LeVan[25], Yang et al[26], Saha et al[27] have shown that the heat of adsorption released makes the adsorption process non-isothermal and imposes a higher regeneration temperature after equilibrium hence removing this heat potentially can offer improved adsorption process.

The objective of this paper is to evaluate the experimental thermal performances of the HCOHPs in order to ascertain their heat transfer capabilities and performance. The HCOHPs, designed with their evaporators and condensers coiled for wider surface area coverage around a packed bed vessel for passive heat transfer, were filled with ethanol, methanol and deionised water respectively and tested under laboratory conditions.

2. Experimental Setup and Procedure

2.1. Physical Model Description

The physical model of the HCOHP in Figure 1 shows helically coiled condenser and evaporator sections with an inlet valve for charging with working fluid on one of the adiabatic sections. The helically coiled evaporator section allows for the slotting of the cylindrical copper vessel through for heat transfer between the walls of the vessel and the evaporator of the HCOHP. The condenser section offers a similar surface area for heat exchange between the surrounding ambient environment.

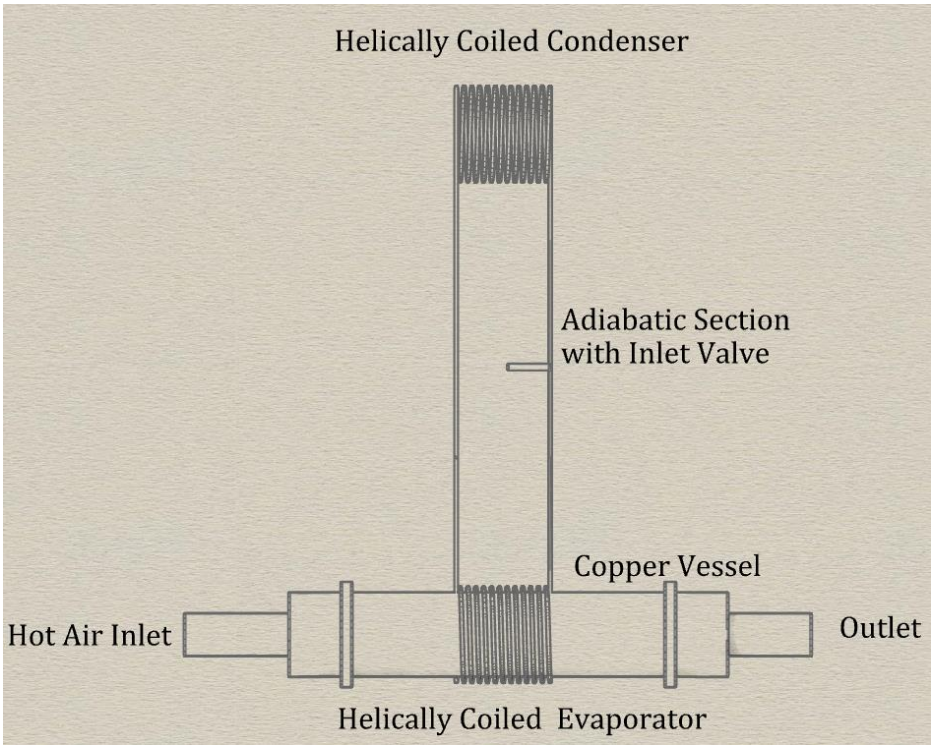

Figure 1 Physical model of the HCOHP Oriented Vertically

2.2. HCOHP Development

The working fluid in the HCOHP forms liquid slugs and vapour plugs in the entire tube, as the diameter of the pipes did not exceed the critical diameter[28-29]. Since surface tension predominates the two-phase flow in the HCOHPs, the inner diameters satisfied[30] equation (1).

$$D_{crit} = 2L = 2\sqrt{\frac{\sigma}{g(\rho_l - \rho_v)}} \quad (1)$$

The HCOHPs were fabricated out of copper pipe of internal diameter 2mm determined in accordance with the criteria established in equation (1). Table 1 shows the general dimensions of the HCOHP. To enhance the heat transfer rate and sustain higher heat loads without dry-out, the evaporator length of the HCOHPs were no larger than that of the condenser[30] and determined using equation (2).

$$L_{eff} = \frac{1}{2}(L_e + L_c) + L_a \quad (2)$$

Table 1 HCOHP Dimensions

Parameter	Value	Units
Inner Diameter	2	mm
Thickness	1	mm
Diameter of Coil	8	cm
Length of Compressed Coil	10	cm
Number of Turns	10	-
Length of Adiabatic Section	20	cm
Total Length of HCOHP	38	cm

To ensure that vacuum can be created within them, the HCOHPs were pressure tested using a DynAir compressor where a maintained pressure of about 3bar (~41 psi) was recorded. Khandekar et al[31] for instance fitted a T-connector on a pulsating heat pipe (PHP) with a filling/metering valve, tested the final assembly under vacuum, and found that a pressure of 10^{-4}mbar could be easily maintained. Ethanol, methanol and water were selected as suitable working fluids for the HCOHPs useful in the temperature range of the adsorption packed bed system to be integrated with. Their merit number[32], M, a convenient means of comparing working fluids determined from equation (3) and other standard thermophysical properties at 30°C are presented in Table 2.

$$M = \frac{\rho_l \lambda \sigma}{\mu_l} \quad (3)$$

Table 2 Thermophysical Properties and Figure of Merit for the Selected Working Fluids

Working Fluid	Temperature, °C	Density (kg/m³), ρ_l	Latent Heat of Evaporation(kJ/kg), λ	Surface Tension (N/m), σ	Liquid Viscosity (cP), μ_l	Figure of Merit M (W/m²)	Comments
Ethanol	30	781	888.60	0.024	1.02	1.6×10^7	Figure of merit calculated with data from Reay et al[33]
Methanol	30	782	1155.00	0.022	0.52	3.78×10^7	
Water	30	996	2430.50	0.071	0.80	2.15×10^8	

Before charging the HCOHPs with working fluid, they were evacuated by a maximum pressure of about 0.1MPa using a vacuum pump under standard atmospheric pressure of approximately 101,325Pa. They were then weighed empty and their individual masses recorded. Once evacuated, the HCOHPs were fully charged using a syringe and the volume recorded. The fully charged HCOHPs were then weighed again and evacuated completely using the vacuum pump before filling to about 60% volume using a syringe under ambient room temperature and atmospheric pressure (see Table 3 for charging data). According to Senjaya and Inoue[34] high heat transfer rate occurs when HCOHPs are charged at the optimum filling ratios (about 50–60%), which are higher than those of conventional heat pipes.

Table 3 HCOHP Working Fluid Charging Data							
Heat Pipe	**Working Fluid**	**Dry HCOHP Weight, kg**	**HCOHP Weight @ ~60% Filled Volume, kg**	**Mass of Working Fluid in HCOHP, kg**	**Fully Filled Volume, ml**	**Partially Filled (~60%) Volume, ml**	**Evacuation Pressure, MPa**
EOHP 1	Ethanol	0.68	0.70	0.017	~26	~16	~0.0013
EOHP 2	Ethanol	0.67	0.68	0.012	~26	~16	~0.0013
EOHP 3	Ethanol	0.68	0.70	0.012	~26	~16	~0.0013
MOHP 1	Methanol	0.68	0.69	0.012	~26	~16	~0.0013
MOHP 2	Methanol	0.68	0.69	0.012	~26	~16	~0.0013
MOHP 3	Methanol	0.68	0.69	0.014	~26	~16	~0.0013
WOHP 1	Deionized Water	0.64	0.66	0.019	~26	~16	~0.0013
WOHP 2	Deionized Water	0.64	0.65	0.011	~21	~12.6	~0.0013
WOHP 3	Deionized Water	0.64	0.66	0.021	~25	~15	~0.0013

2.3. Data Collection and Analysis Approach

OMEGA k-type thermocouples were connected to the condensers, evaporators and adiabatic sections and then connected to a Yokogawa DX 200 data logger and a desktop computer for the collection of temperature data. The evaporator sections were then subjected to varied heat input with the condensers exposed to the ambient surroundings. Since the HCOHPs are to fit around a cylindrical copper vessel of solid desiccants, testing was carried out with hot air blown into same copper vessel and the heat generated via the walls transferred to the helically coiled evaporators as shown in Figure 2. For this approach three test runs, Run 1 or (R1), Run 2or (R2) and Run 3 or (R3) were respectively carried out at various heat inputs testing the limits of the HCOHPs. In other studies, Pachgharea and Mahalleb[35] recorded the temperature of their PHP by fixing three K-type thermocouples to the evaporator, condenser and adiabatic sections respectively. Sriudom et al[36] also collected temperature data from their Helical Oscillating Heat Pipe using 12 type K-thermocouples with ±1.5°C accuracy and a Yokogawa DX 200 data logger with ±1°C accuracy. Lin et al[37] used OMEGA K-type thermocouples to measure the wall temperature at different positions on the outer wall of their MOHPs.

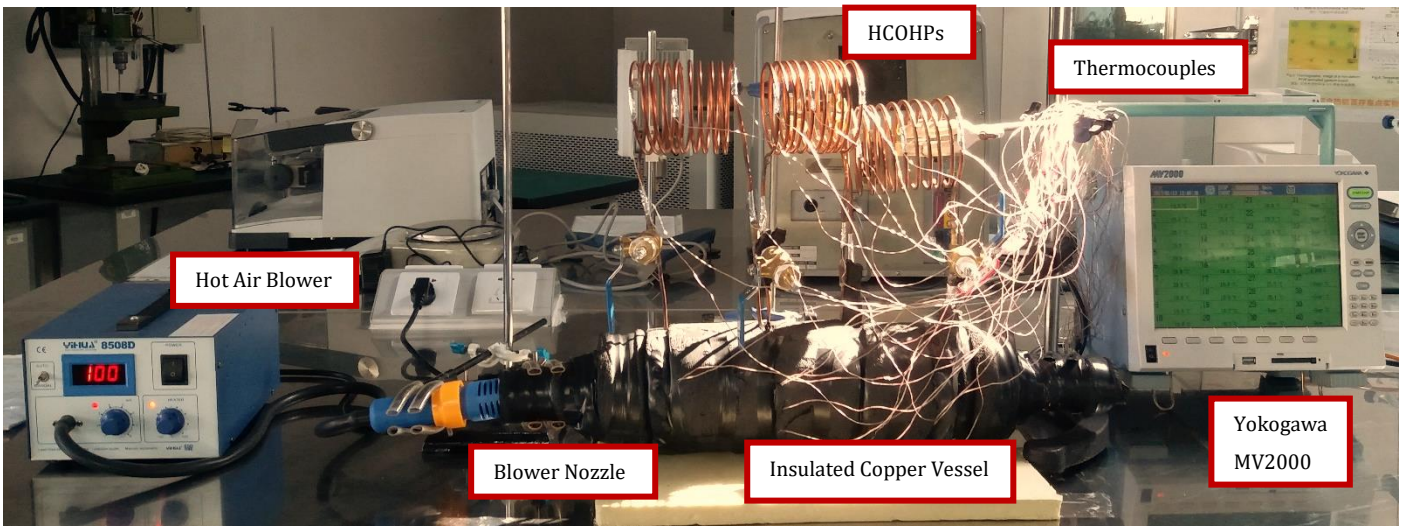

Figure 2 HCOHP Experimental Setup in the Laboratory

The HCOHPs were oriented vertically with the evaporators at the bottom and the condensers at the top. To ensure that the heat input conditions are the same for all the HCOHPs, the integrated section was insulated using a 20mm thick nitrile rubber thermal insulation material. Thermocouples attached to the inner and outer wall surfaces of the cylindrical copper vessel provided the temperature readings of the inner and outer surface for the determination of the input flux and power. To ensure the HCOHPs were tested under the same conditions, the ethanol based OHP (EOHP), methanol based OHP (MOHP) and water based OHP (WOHP) were all integrated together with the empty cylindrical copper vessel for heat input under same conditions for each test run. The evaporator section and cylindrical copper vessel dimensions relevant for the heat transfer calculations are presented in Tables 4 and 5.

Table 4 Evaporator Dimensions

Parameter	Value	Units	Comments
Area of Evaporator, A_e	0.02	m^2	From design parameters
Length of Evaporator, L	0.19	m	From design parameters

Table 5 Dimensions of the Heat Transfer Vessel

Component	Total Length (cm)	Inner Diameter (cm)	Outer Diameter (cm)
Copper Vessel	30.00	7.80	8.00

3. Results and Discussions

The experiments were conducted under ambient room temperature corresponding to the initial temperatures of the condensers for each test run and ambient pressure of about 102.0Bar. The data sampling time was 5.00s and each test lasted for about 1600s.

3.1. Heat Transfer from Cylindrical Copper Vessel

The cylindrical copper vessel was pushed through the helically coiled evaporators of the HCOHPs for testing. This was done to ensure the power input and test conditions were the same for each test run. The three test runs were carried out with the hot air blower set to element temperatures of 100, 125 and 192°C respectively representing test Run 1 or (R1), Run 2 or (R2) and Run 3 or (R3). The rate of heat transfer though the walls of the empty vessel integrated with the HCOHPs is given by equation (4)[38].

$$q_w = -kA_s\frac{dT}{dr} = 2\pi \mathrm{L}k\frac{T_i - T_o}{\ln\left(r_o/r_i\right)} \quad (4)$$

The output heat flux from the cylindrical copper vessel for the test runs was then determined from equation (4) along with the temperature difference between the outer and inner surfaces of the cylindrical copper vessel obtained using the K-type thermocouples. The corresponding output power from the cylindrical copper vessel was then determined by multiplying the area covered by each HCOHP evaporator section by the heat flux into that section. Averages of the output heat flux and corresponding output power obtained from the cylindrical copper vessel are presented in Table 6.

Table 6 Average Vessel Heat Power and Output Heat Flux

Run	Average Heat Flux (W/m^2)	Average Power (W)
R1	21166.80	719.67
R2	21734.23	738.96
R3	35993.40	1223.78

3.2. Thermal Contact Resistance

The differences in vessel heat flux and evaporator heat flux was largely attributed to the thermal contact resistance between the evaporator walls and the walls of the cylindrical copper vessel. To determine the thermal contact resistance, the average heat flux on the interfaces where the temperature jump occurred were determined. In practice, thermal contact resistances exists at contact interfaces of the exterior surface of a heat pipe and the system with which it is in contact with for the heat transfer[39]. In this present study, the interface between the evaporator coils of the HCOHPs and the cylindrical copper vessel integrated with presented some thermal contact resistance to the heat transfer. The thermal resistance between two contacted solid surfaces of the evaporator coils and the walls of the cylindrical copper vessel resulting from the surface irregularities and asperities was calculated using equations (5 and 6) obtained from Zhang et al[40].

$$R_c = \frac{T_v - T_{evap}}{q_{av}} \tag{5}$$

$$q_{av} = \frac{q_v + q_{evap}}{2} \tag{6}$$

In Figure 3a-c, transient plots of the thermal contact resistance determined from equations (5 and 6) are presented for the three test runs. The thermal contact resistance for the WOHP was found to be relatively higher compared to the other two HCOHPs. Although the materials in contact were all copper assumed to have relatively similar surface finishing, the variation in the magnitude of the thermal contact resistances was attributed to the three different working fluids in the respective HCOHPs resulting in different effective thermal conductivities at their respective evaporators.

For the EOHP in Figures 3a-c, the trend generally shows a decreasing thermal contact resistance with increasing overall average heat flux. In Figure 3c, instabilities observed for the MOHP in run 3 could be attributed to the increase in overall average heat flux influencing its effective thermal conductivity.

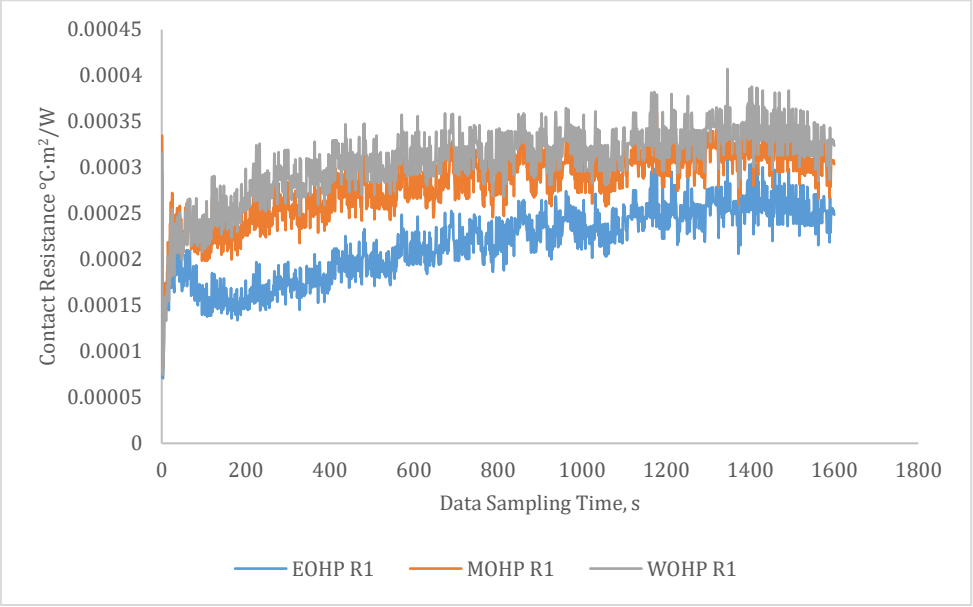

Figure 3a Thermal Contact Resistance for Run 1

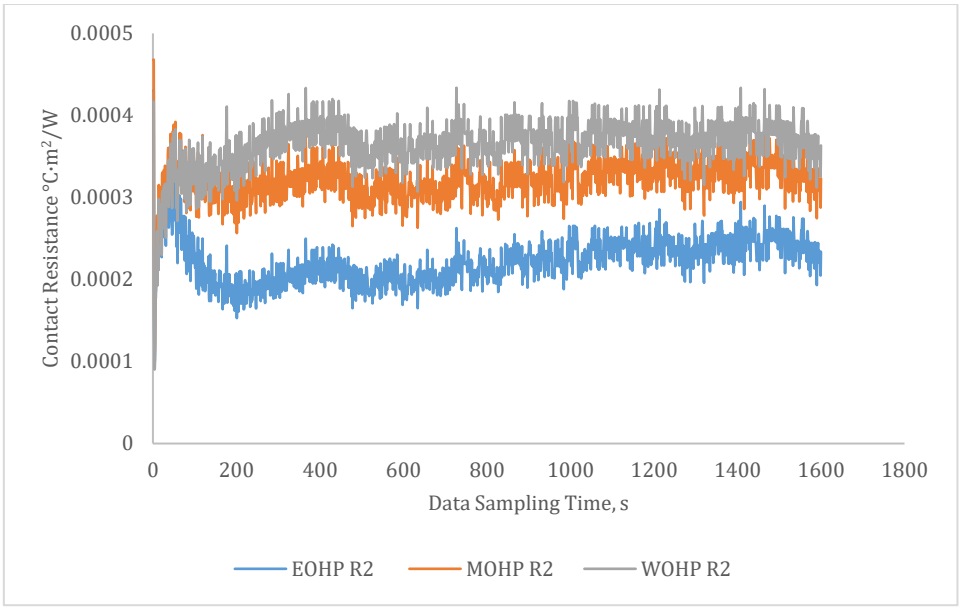

Figure 3b Thermal Contact Resistance for Run 2

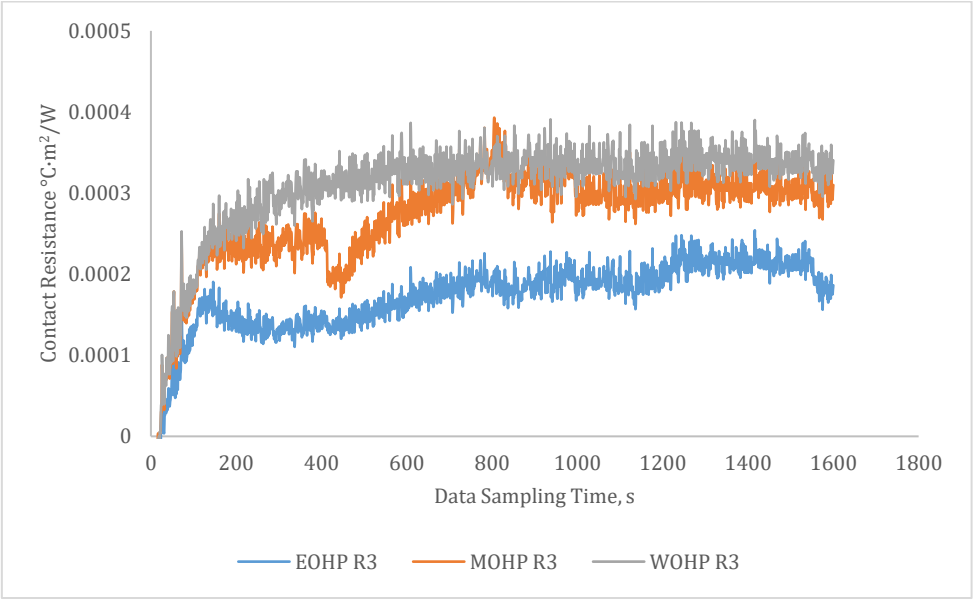

Figure 3c Thermal Contact Resistance for Run 3

Table 7 shows the overall average heat flux and the average thermal contact resistance for each HCOHP under the three test conditions. The average results show the thermal contact resistance varied with the working fluid type in the HCOHP and also the average heat flux. The average heat flux of the vessel and evaporator coils were found to be relatively high for the WOHP and low for the EOHP due to the variation in their effective thermal conductivities. Overall, the thermal contact resistance varied with average heat flux amount and working fluid type.

Table 7 Average Thermal Contact Resistance and Overall Average Heat Flux

HCOHP	***Test Run 1***		***Test Run 2***		***Test Run 3***	
	Thermal Contact Resistance,°C·m²/W	***Heat Flux, W/m²***	***Thermal Contact Resistance, °C·m²/W***	***Heat Flux, W/m²***	***Thermal Contact Resistance, °C·m²/W***	***Heat Flux, W/m²***
EOHP	0.00022	13706.75	0.00022	14156.11	0.00017	22117.24
MOHP	0.00028	15069.72	0.00032	16397.81	0.00027	25592.52
WOHP	0.00031	15625.28	0.00036	17657.71	0.00031	27080.96

3.3. *Heat Input and Output of the HCOHPs*

The evaporator input heat flux was determined using Fourier's Law given by equation (7) and the temperature difference between the cylindrical copper vessel wall and the HCOHP evaporator. Although the output heat flux from the cylindrical copper vessel was found to be relatively the same at each point on the vessel for each respective test run, the evaporator heat fluxes varied. Since the integration of the HCOHPs' evaporators and cylindrical copper vessel required heat to be transferred via their walls through conduction, there was thermal contact resistance (TCR) which caused a temperature jump at the contact interface[42]. Average heat fluxes of 6246.71W/m^2, 8972.64W/m^2 and 10083.76W/m^2 were obtained for R1; 6577.99W/m^2,11061.40W/m^2 and 13581.18W/m^2, for R2; and 8241.08W/m^2, 15191.64W/m^2 and 18168.52W/m^2 for R3 all respectively for EOHP, MOHP and WOHP for each test run. And from these results, the WOHP evaporator had a relatively higher evaporator heat flux in all three test runs. The power input at the evaporator was determined using the area of the evaporator section presented in Table 4 multiplied by the evaporator wall heat flux input. The evaporator wall heat flux was calculated using the Fourier's Law given by equation (7)[41].

$$Q = -kA\frac{dT}{dx} \tag{7}$$

The temperature difference between the condensers and the ambient surrounding air was used in calculating the condenser heat flux and subsequently heat output power respectively, similar to the evaporator heat flux and input power determined using equation (7) and Table 4. For Run 1, average condenser output heat fluxes of 2388.75 W/m^2, 2495.37W/m^2 and 2599.80W/m^2 were obtained for the EOHP, MOHP and WOHP respectively. For Run 2 the average heat fluxes were 2417.36W/m^2, 2435.52W/m^2 and 2884.70W/m^2 whilst for Run 3 they were 6126.14W/m^2, 7385.52W/m^2 and 7759.94W/m^2 all respectively for the EOHP, MOHP and WOHP.

In Figures 4a-c, transient results of the heat output from the evaporators and condensers of the HCOHPs are presented. The power input for the WOHP was found to be comparatively higher with the EOHP having the lowest power input to its evaporator. The variation in the effective thermal conductivities as a result of the varied thermophysical properties of the working fluids resulted in the variation of the heat input and outputs for the HCOHP evaporators and condensers. For all three test runs, the power input to the evaporators gradually increased till a relatively steady state condition was attained. The corresponding heat output profiles for the condensers shows a steady increase of condenser heat output with increasing evaporator heat input. Although there were distinct heat input amounts to the evaporators regardless of the fact that the copper vessel integrated generated common output flux for them, the variation in heat output at the corresponding condensers were slight mainly with Figures 4a and b. In Figure 4c, there were significant differences observed for the condenser outputs of the EOHP and MOHP. For the evaporator of the MOHP in Figure 4c, significant variabilities were observed in its evaporator heat input power between 400-1000s. However, its corresponding condenser showed only a blip in the heat output around 800s. It therefore appears that at that heat input power, the evaporator was possibly experiencing dry-out of the working fluid.

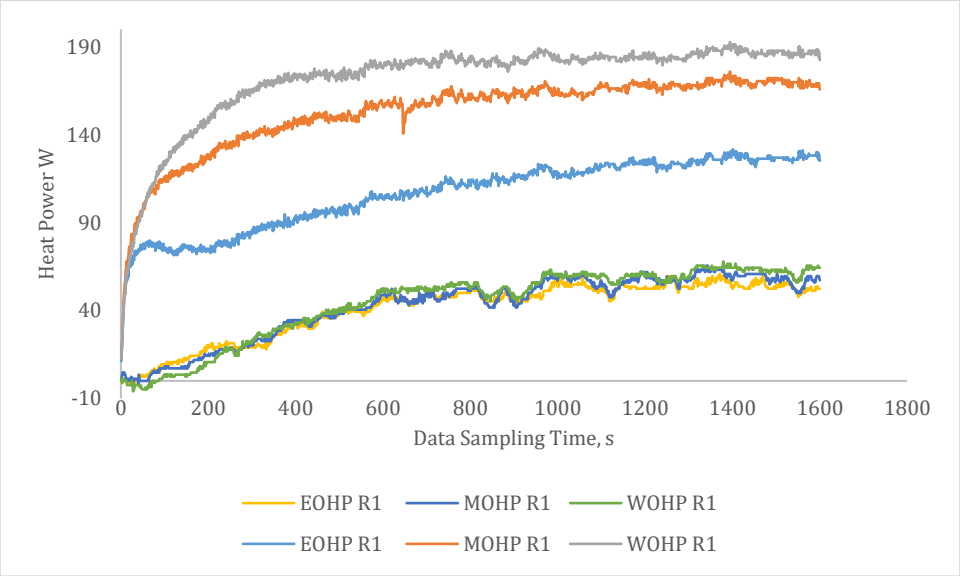

Figure 4a Evaporator Heat Input and Condenser Heat Output Power for Run 1

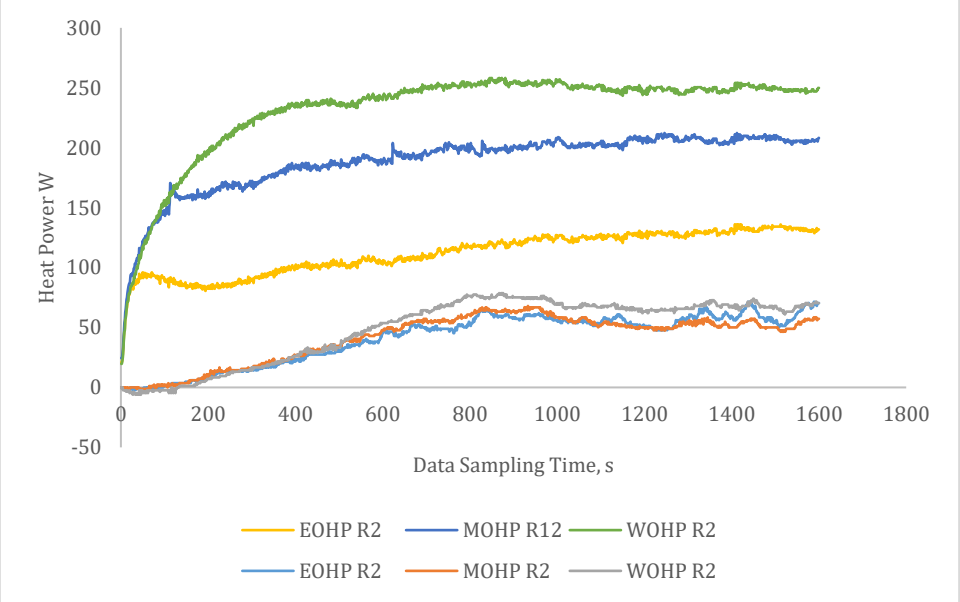

Figure 4b Evaporator Heat Input and Condenser Heat Output Power for Run 2

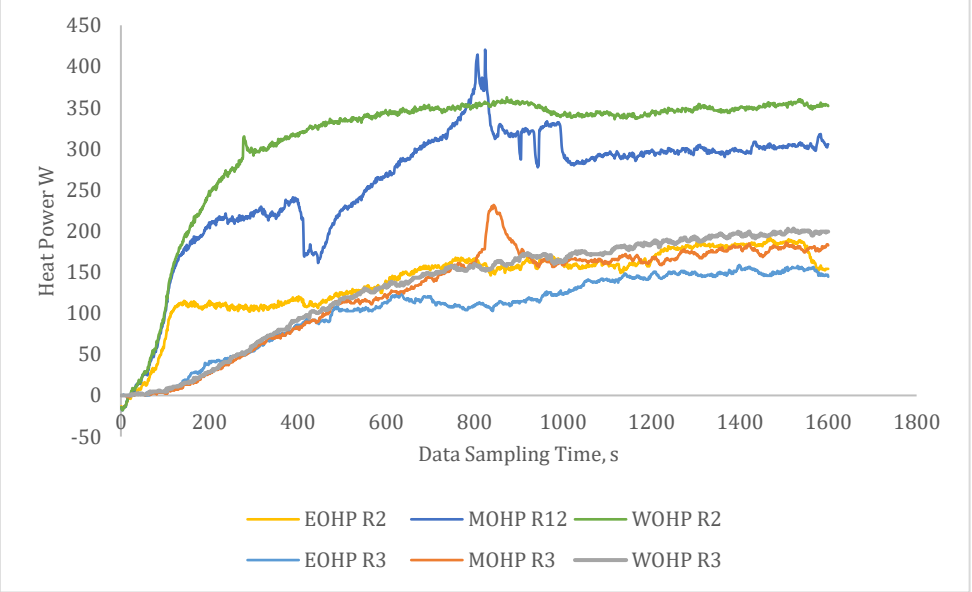

Figure 4c Evaporator Heat Input and Condenser Heat Output Power for Run 3

3.4. Effects of Input Heat Power on HCOHP Evaporator-Condenser Temperature Difference

The evaporator and condenser temperature data were obtained directly using Omega K-type thermocouples. Each test run was commenced at ambient room temperature corresponding to the initial temperature at the condenser sections. The evaporator sections of the HCOHPs integrated with the cylindrical copper vessel were insulated to ensure uniform heat input conditions for each test run. Even though the heat output from the copper vessel was relatively constant for respective test runs, the evaporator heat input amounts for each HCOHP varied as a result of the working fluids varying their respective effective thermal conductivities. Karthikeyan et al[39] also found the effective thermal conductivity of their closed loop pulsating heat pipe varied with heat power for different working fluids. In Figure 5a-c, the evaporator heat input for the WOHP was found to be comparatively larger overall to that of the MOHP and EOHP for similar temperature differences. The EOHP on the other hand required a rather low evaporator heat input for relatively similar evaporator-condenser temperature difference meaning it showed a comparatively low heat transport capability. In Figure 5a, the increasing evaporator-condenser temperature difference with heat load signified the onset of working fluid dry-out. Zhu et al[42] found out that dry-out commenced when the temperature difference between the evaporator and condenser increased.

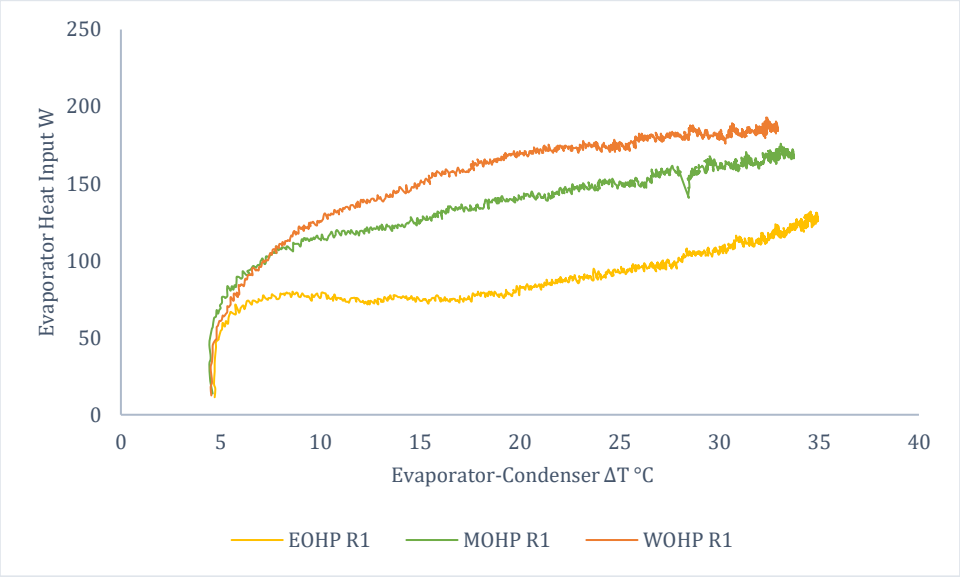

Figure 5a HCOHP Evaporator-Condenser Temperature Difference for Run 1

In Figure 5b, it is observed that as the evaporator heat input increased, so did the evaporator-condenser temperature difference. Here too, the EOHP required a relatively lower evaporator heat input to attain the same evaporator-condenser temperature difference as the WOHP and MOHP. For the MOHP and WOHP, a relatively similar evaporator-condenser temperature difference was attained till the evaporator heat input power increased beyond 160W.

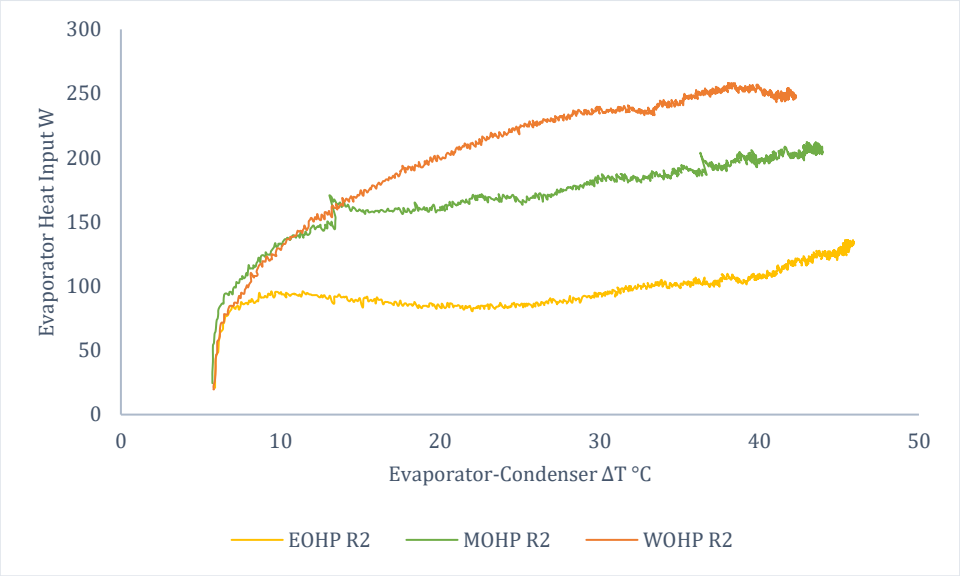

Figure 5b HCOHP Evaporator-Condenser Temperature Difference for Run 2

In Figure 5c, the evaporator-condenser temperature difference also increased with increasing heat input. Here, significant instabilities were observed for the MOHP beyond 234W. The maximum and minimum evaporator heat input values of about 420W and 165W respectively were observed. These instabilities could be attributed to irregular temperature drops at the contact surface between the evaporator of the MOHP and the walls of the copper vessel at the onset of dry-out. Since at the point the liquid phase of the working fluid may be transitioning in the drying out stage, there was the likelihood of evaporation and condensation occurring irregularly, subsequently influencing the effective thermal conductivity at the evaporator section. Fletcher[43] showed that the magnitude of the contact conductance is a function of a number of parameters including the thermophysical and mechanical properties of the materials in contact, the characteristics of the contacting surfaces, the presence of gaseous or nongaseous interstitial media, the apparent contact pressure, the mean junction temperature, and the conditions surrounding the junction. According to Xian et al[44] due to the existence of gaps and spots between contact surfaces, the heat transfer across the interface occurs through a combination of three modes, including point-to-point micro contacts, convection and radiation, causing an additional resistance and temperature drop at the interface.

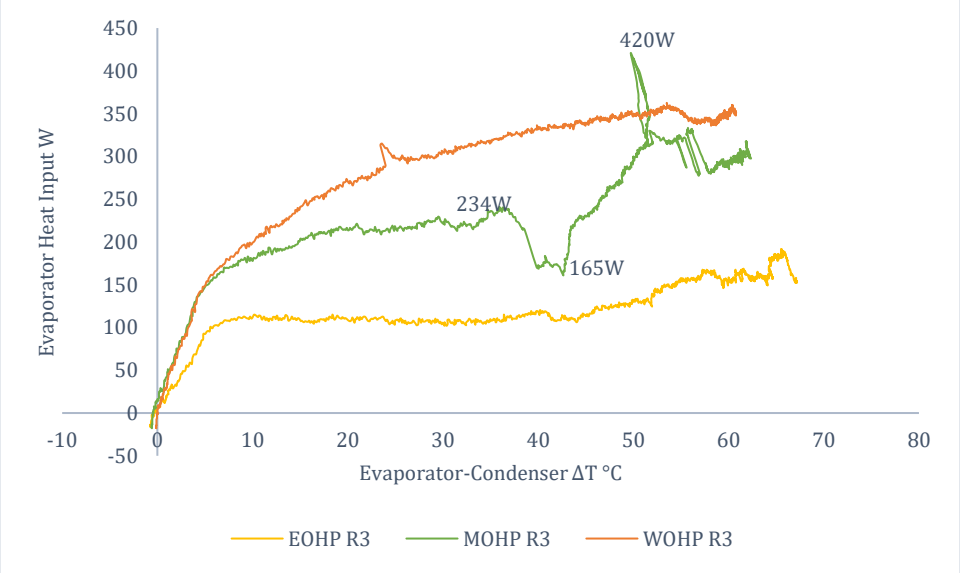

Figure 5c HCOHP Evaporator-Condenser Temperature Difference for Run 3

Overall, the evaporator-condenser temperature differences observed for the HCOHPs increased with increasing evaporator heat input. The WOHP realized similar evaporator-condenser temperature differences at comparatively higher evaporator heat input than MOHP and the MOHP at a relatively higher evaporator heat input than the EOHP. The variation in the temperature difference with heat input was mainly due to the thermophysical properties of the working fluids influencing the effective thermal conductivities of the HCOHPs.

3.5. Overall Thermal Resistance

The overall thermal resistance is the criteria used in evaluating the thermal performance of OHPs[45]. Here the lower the value the better the performance. The HCOHPs' thermal performances were evaluated by determining the thermal resistance (R) using equation (8) obtained from Hao et al[46].

$$R = \frac{\bar{T}_e - \bar{T}_c}{Q} \tag{8}$$

Figure 6a-c shows thermal resistances of the HCOHPs determined using equation (8) and plotted against the evaporator heat input for all test runs. The results show differences in performance between the HCOHPs at varied heat input. In Figure 6a, the plots show the thermal resistances declined from start-up to a critical evaporator heat input power where it started increasing. As the evaporator heat input increased beyond 60W, differences in performance were observed. For the EOHP, its thermal resistance sharply increased when the evaporator heat input power reached about 70W, representing the onset of dry-out of the ethanol working fluid in the evaporator. The thermal resistances for the MOHP and WOHP on the other hand increased gradually from a critical evaporator input power of about 105W at which point the onset of dry-out was observed. According to Zhu et al[47] at the onset of dry-out, the temperature difference between the evaporator and condenser widens, causing an increase in the thermal resistance. At an average cylindrical copper vessel heat flux of 21166.80W/m^2 for test run 1, the EOHP evaporator power was limited to a maximum of 131W, whilst that of the MOHP and WOHP were limited to 173W and 192W respectively. This was as a result of the working fluids influence on the effective thermal conductivity of the HCOHPs subsequently imposing a heat transfer limit.

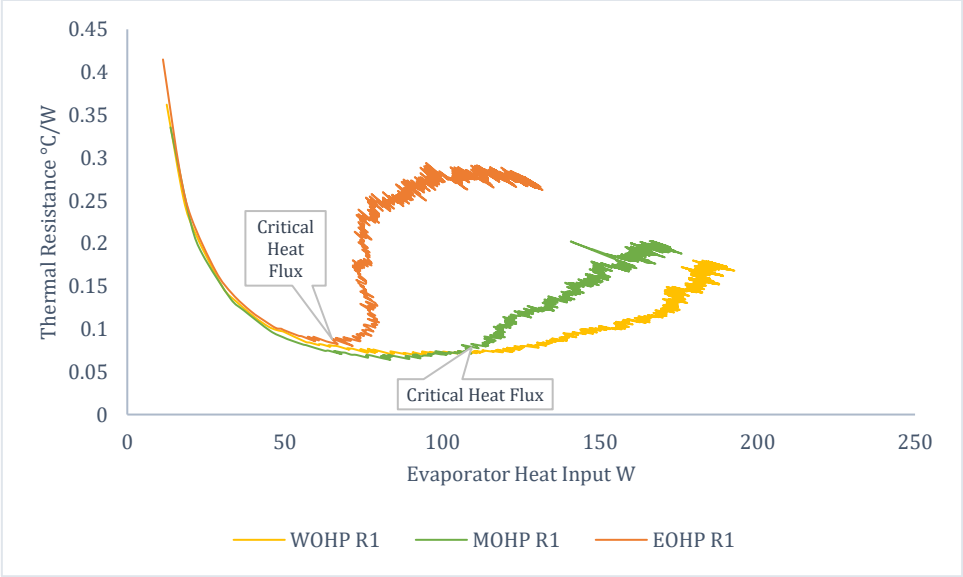

Figure 6a HCOHP Thermal Resistance for Runs 1

Figure 6b shows the performance of the three HCOHPs under test run 2. Under this test condition, the thermal resistance of the EOHP increased sharply when the evaporator heat input power increased beyond 83W. For the MOHP and the WOHP, their thermal resistances increased gradually from a critical evaporator input heat power of 135W. Comparing

to Figure 6a, it is evident that the critical evaporator heat input power observed to be the onset of dry-out changed under this test run. For an average output flux of 21734.23 W/m² from the cylindrical coper vessel, the EOHP attained a maximum evaporator input power of about 134W, whilst that for the MOHP and WOHP were 210W and 256W respectively. Beyond the 83W, the performance of the EOHP declined significantly with dry-out commencing. For the MOHP and WOHP, both were able to effectively perform well below 161W beyond which their performances comparatively started declining and the onset of dry-out begun.

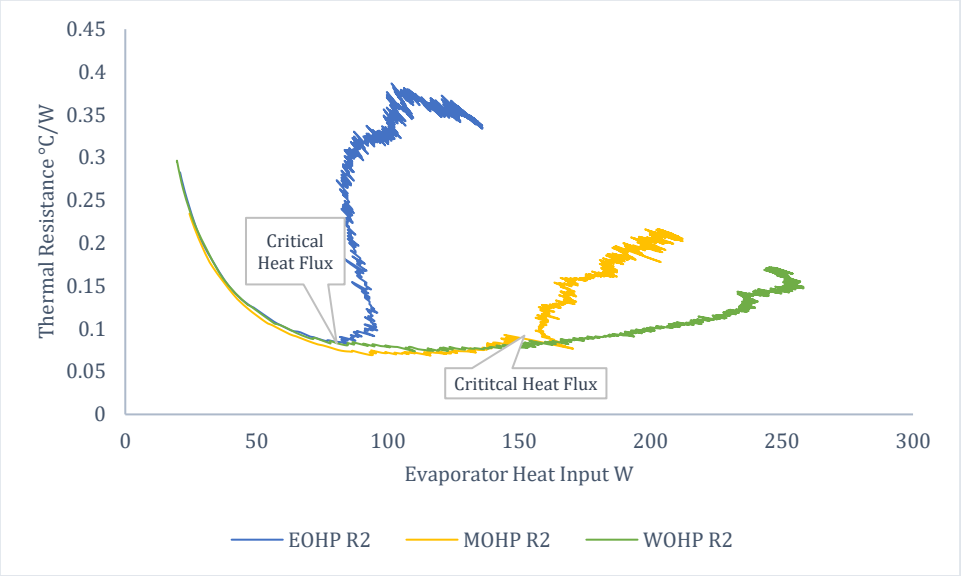

Figure 6b HCOHP Thermal Resistance for Run 2

In Figure 6c, there were perturbations at start-up due to the relatively large amount of heat input for this test run. For the EOHP, the thermal resistance was relatively steady until at about 98W when it sharply increased and dry-out commenced. For the WOHP, the profile was similar to the profiles presented in Figures 6a and b only beginning it ascent around 160W towards dry-out. For the MOHP, onset of dry-out was also around 160W however instabilities were experienced after evaporator input heat power went beyond 234W affecting its performance.

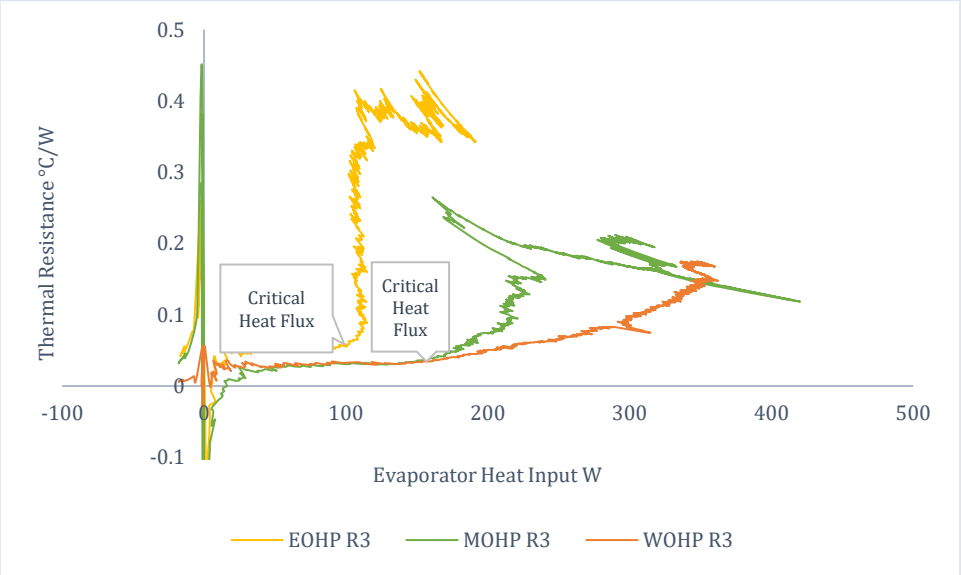

Figure 6c HCOHP Thermal Resistance for Run 3

Increasing the heat load is found to increase the driving pressure difference in OHPs resulting in changes in the fluid motions from small oscillation to bulk ones reaching circulation subsequently triggering a decrease in the overall thermal

resistance[48]. However, as observed in Figure 6a-c beyond the critical heat flux, dry-out commenced resulting in a decrease in HCOHP thermal performance. This was because the increase in the heat input led to the dearth of liquid quantity in the evaporator section subsequently drying out the liquid film inside the evaporator tube surface[49].

It is important to note that, the HCOHPs investigated are essentially single turn closed loop oscillating heat pipes with their evaporator and condenser sections helically coiled to fit around the horizontal copper vessel. The helically coiled evaporator and condenser sections coupled with the vertical orientation of the HCOHPs potentially gives the evaporators the capacity to hold more working fluid. As shown by Sriudom et al[16], the characteristics of the helical coil such as the pitch distance influences flow pattern percentage with an increased in pitch distance increasing stratified wavy flow pattern percentage in helical OHPs. According to Khandekar et al[50], the performance independence of Closed Loop Pulsating Heat Pipes (CLPHP) with orientation is affected by the number of turns. Khandekar and Groll[51] explained that if the number of turns of a CLPHP is small, then the heat handled by each turn will be quite high. If it is increased (keeping the filling ratio constant) with the heater power fixed, then the net heat handled by each CLPHP turn reduces. Mameli et al[52] found that bends and turns influences local pressure losses which affects the operation of Closed Loop Pulsating Heat Pipes (CLPHP) especially in the horizontal mode and for high heat input levels. From the test results in Figures 6a-c, it can be resolved that the HCOHPs capacity to manage these relatively large amounts of heat input were due to the helically coiled sections creating comparatively larger evaporator sections holding relatively more working fluid than the conventional serpentine single turn closed loop OHP system of the same volume and fill ratio.

3.6. Experimental Uncertainty Analysis

The fundamental quantity measured was temperature with all other relevant parameters derived. The absolute uncertainty of the temperature measurement from the thermocouples was ±0.05°C. The percentage uncertainty was determined from $percentage\ Uncertainty = \frac{Absolute\ Uncertainty}{Measured\ Value} \times 100\%$. Averages of the percentage uncertainty measurement for the temperature are presented in Table 8. The values obtained were relatively lower in the evaporators than in the condensers. Between respective evaporators and condensers there was a slight variation in the uncertainty measurement under all the test conditions. The uncertainty in the temperature measurement in the evaporators was observed to improve marginally with increasing heat input flux, whilst in the condensers the average percentage uncertainty remained relatively the same.

Table 8 Average Percentage Uncertainty Temperature Measurement (%)

Test Run	**EOHP**		**MOHP**		**WOHP**	
	Evaporator	*Condenser*	*Evaporator*	*Condenser*	*Evaporator*	*Condenser*
R1	0.22	0.52	0.23	0.52	0.23	0.52
R2	0.19	0.51	0.19	0.51	0.20	0.50
R3	0.18	0.51	0.19	0.50	0.19	0.51

The thermal resistance, the measure of the thermal performance of the HCOHPs is a derived quantity. In Table 9, its mean, standard deviation and standard error of its mean are presented.

The mean[53] was determined from equation (9)

$$\bar{X} = \frac{\Sigma X}{N} \quad (9)$$

The standard deviation[53] was determined by equation (10)

$$s = \sqrt{\frac{\sum(X-\bar{X})^2}{N}} \tag{10}$$

The estimate of the standard error of the mean[53] is given by equation (11)

$$S_{\bar{x}} = \frac{s}{\sqrt{N}} \tag{11}$$

Bar, EOHP R3, the standard deviation was marginally small and decreased by 2 orders of magnitude. The estimated standard error of the mean for the thermal resistance of all the HCOHPs under the test conditions was inconsequential from the values in Table 9.

Table 9 Uncertainty Analysis of HCOHP Experimental Thermal Resistance

Test Run		**Thermal Resistance (°C/W)**		
		EOHP	**MOHP**	**WOHP**
R1	Mean	0.26	0.17	0.15
	Standard Deviation	0.05	0.04	0.03
	Standard Error of the Mean	0.0013	0.0010	0.0008
R2	Mean	0.33	0.18	0.14
	Standard Deviation	0.07	0.04	0.03
	Standard Error of the Mean	0.0018	0.0010	0.0008
R3	Mean	0.33	0.16	0.13
	Standard Deviation	0.12	0.07	0.05
	Standard Error of the Mean	0.0030	0.0018	0.0013

3.7. Error Analysis

The experimental results obtained depended on several influencing factors that affected its precision and accuracy. Using the theoretical study as the benchmark, the fabricated device with its welded joints and valve connections was slightly different from the theoretical model. In the measurement of the mass of the three HCOHP devices and the volume of the working fluid therein (See Table 3), slight differences resulting from imperfections in the fabrication process was observed. In the charging of the HCOHPs with working fluid, the theoretical assumption was that the evacuated HCOHP devices maintained their evacuation pressure whilst being charged with working fluid. Although care was taken towards achieving that, its 100% certainty was to some extent doubtful. The working fluid, deionized water manufactured from an in-house plant in the laboratory was assumed to be free of non-condensable gases and was not degassed before charging the HCOHPs.

In the testing of the HCOHPs, they were fitted around the cylindrical copper vessel based on the assumption that all inner coil surfaces of the evaporator section were uniformly in contact with the outside walls of the cylindrical vessel. The temperature data collected was sampled at the minimum 5.00s interval for the setup to capture the oscillations in the measurement. However, earlier data collected with sample interval of 10.00s presented no difference in the results demonstrating either the sensitivity of the thermocouples used or the Yokogawa MV2000's capacity to capture the temperature signal within much smaller intervals.

4. Conclusion

The thermal performance of a novel helically coiled oscillating heat pipe (HCOHP) for isothermal adsorption has been experimentally investigated. The results show that;

- Between the respective helically coiled copper evaporators and the copper vessel, the thermal contact resistance (TCR) was found to typically vary with working fluid type owing to their respective effective thermal conductivities. The TCR observed at each respective average input heat flux was higher for the WOHP and correspondingly lower for the EOHP.
- There was a critical heat flux at each evaporator beyond which the thermal resistance started increasing and there was the onset of dry-out. This critical heat flux was observed to vary with heat input amount at the evaporator and also working fluid type. For the EOHP, the critical heat fluxes were 70W, 83W and 98W respectively for R1, R2 and R3, whilst for both MOHP and WOHP they were 105W, 135W and 160W for the respective test runs. The rise in thermal resistance at those critical heat fluxes was observed to be gradual for the MOHP and WOHP and sharp for the EOHP.
- Performance instabilities were observed for the MOHP beyond 234W owing to the possibility of the liquid phase of the working fluid transitioning in the drying out stage and subsequently influencing the effective thermal conductivity at the evaporator section.

The experimental evaluation showed that the HCOHPs were capable of managing relatively large amounts of heat input than the conventional serpentine single turn closed loop OHP system with the WOHP type achieving the best performance under all tested condition. We believe the next step for this investigation should involve the visualization of the internal flow dynamics in order to fully understand the influence of the configuration on overall performance.

Nomenclature

- A = cross sectional area, m^2
- A_s=surface area of cylindrical copper vessel (m^2)
- D_{crit} = critical diameter (m)
- g = acceleration due to gravity (m/s^2)
- h = heat transfer coefficient ($W/m^2 \cdot °C$)
- k = material thermal conductivity ($W/m \cdot K$)
- L = length l (m)
- N=sample size
- Q = heating power input (W)
- q_{av} =the average heat flux of the vessel and evaporator coils (W/m^2)
- q_v = heat flux from the vessel (W/m^2)
- q_{evap} = heat flux at the evaporator (W/m^2)
- R = thermal resistance (°C/W)
- r_i=inner radius of packed bed vessel (m)
- r_o=outer radius of packed bed vessel (m)
- s=standard deviation
- $S_{\bar{x}}$= standard error of the mean

- t= time (s)
- T_i=inner surface temperature of packed bed vessel (K)
- T_o=outer surface temperature of packed bed vessel (K)
- T_v =the surface temperatures of vessel at the contact interface (°C)
- T_{evap} =the surface temperatures of evaporator coils at the contact interface (°C)
- T = temperature (K or °C)
- ΔT = temperature difference (K)
- u = velocity magnitude (m/s)
- X= sample
- $\bar{X}$= sample mean

Greek Letters

- ρ = density (kg/m^3)
- σ = surface tension (N/m)

Subscripts

- a = adiabatic
- c = condenser
- e = evaporator
- eff = effective
- ext = external
- f = fluid
- l = liquid
- v = vapour
- W = Wall

Abbreviations

- EOHP – Ethanol Oscillating Heat Pipe
- HCOHP- Helically Coiled Oscillating Heat Pipe
- MOHP - Methanol Oscillating Heat Pipe
- R1 – Run 1
- R2 – Run 2
- R3 – Run 3
- TCR – Thermal Contact Resistance
- WOHP- Water Oscillating Heat Pipe

Reference

1. Akachi, H. (1990) “Structure of a heat pipe”, U.S. Pat., 4921041.

2. Zhang, Yuwen and Faghri, Amir (2008) 'Advances and Unsolved Issues in Pulsating Heat Pipes', Heat Transfer Engineering, 29:1, 20 – 44

3. Lin, Zirong. Wang, Shuangfeng. Huo, Jiepeng. Hu, Yanxin. Chen, Jinjian. Zhang, Winston and Lee, Eton (2011) Heat transfer characteristics and LED heat sink application of aluminum plate oscillating heat pipes. Applied Thermal Engineering, Volume 31, Issues 14–15, Pages 2221-2229

4. Bhuwakietkumjohn, N. and Rittidech, S. (2010) Internal flow patterns on heat transfer characteristics of a closed-loop oscillating heat-pipe with check valves using ethanol and a silver nano-ethanol mixture. Experimental Thermal and Fluid Science, Volume 34, Issue 8, Pages 1000-1007

5. Bejan, Adrian. and Kraus, Allan D. (2003). Heat Transfer Handbook. John Wiley & Sons.

6. Ma, H. B. Borgmeyer, B. Cheng, P. and Zhang, Y. (2008) Heat Transport Capability in an Oscillating Heat Pipe. J. Heat Transfer 130(8), 081501 (May 29, 2008) (7 pages) doi:10.1115/1.2909081

7. Song, Yanxi. and Xu, Jinliang. (2009) Chaotic behaviour of pulsating heat pipes. International Journal of Heat and Mass Transfer, Volume 52, Issues 13-14, Pages 2932-2941

8. Richardson, J. T., Paripatyadar, S. A. and Shen, J. C. (1988), Dynamics of a sodium heat pipe reforming reactor. AIChE J., 34: 743–752. doi:10.1002/aic.690340505

9. Jouhara, H. Nannou, T.K. Anguilano, L. Ghazal, H. and Spencer, N. (2017) Heat pipe based municipal waste treatment unit for home energy recovery. Energy, http://doi.org/10.1016/j.energy.2017.02.044

10. Swanson, Theodore D. and Birur, Gajanana C. (2003) NASA thermal control technologies for robotic spacecraft. Applied Thermal Engineering, Volume 23, Issue 9, Pages 1055-1065

11. Tseng, Chih-Yung. Yang, Kai-Shing. Chien, Kuo-Hsiang. Jeng, Ming-Shan. and Wang, Chi-Chuan. (2014) Investigation of the performance of pulsating heat pipe subject to uniform/alternating tube diameters. Experimental Thermal and Fluid Science, Volume 54, Pages 85-92

12. Liu, S., J. Li, et al. (2007). "Experimental study of flow patterns and improved configurations for pulsating heat pipes." Journal of Thermal Science 16(1): 56-62.

13. Tong, B.Y., Wong, T.N and Ooi, K.T. (2001) Closed-loop pulsating heat pipe. Applied Thermal Engineering, Volume 21, Issue 18, Pages 1845-1862

14. Qu, Jian. Li, Xiaojun. Cui, Yingying . and Wang, Qian. (2017) Design and experimental study on a hybrid flexible oscillating heat pipe. International Journal of Heat and Mass Transfer, Volume 107, Pages 640-645

15. Chien, Kuo-Hsiang. Lin, Yur-Tsai. Chen, Yi-Rong. Yang, Kai-Shing. and Wang, Chi-Chuan. (2012) A novel design of pulsating heat pipe with fewer turns applicable to all orientations. International Journal of Heat and Mass Transfer, Volume 55, Issues 21–22, Pages 5722-5728

16. Sriudom, Y., Rittidech, S. Chompookham, T. (2015). "The Helical Oscillating Heat Pipe: Flow Pattern Behaviour Study." Advances in Mechanical Engineering 7(1): 194374.

17. Yi, Jie. Liu, Zhen-Hua. and Wang, Jing (2003) Heat transfer characteristics of the evaporator section using small helical coiled pipes in a looped heat pipe. Applied Thermal Engineering, Volume 23, Issue 1, Pages 89-99

18. Nic An tSaoir, Méabh. Fernandes, Daniel Luis Abreu. Jacinto Sá, McMaster, Michael. Kitagawa, Kuniyuki. Hardacre, Christopher. and Aiouache, Farid (2011) Visualization of water vapour flow in a packed bed adsorber by near-infrared diffused transmittance tomography. Chemical Engineering Science, Volume 66, Issue 24, Pages 6407-6423
19. Rady, M.A. Huzayyin, A.S. Arquis, E. Monneyron, P. Lebot, C. and Palomo, E. (2009) Study of heat and mass transfer in a dehumidifying desiccant bed with macro-encapsulated phase change materials. Renewable Energy, Volume 34, Issue 3, Pages 718-726
20. Pentchev, Ivan Paev, Kostadin and Seikova, Ilona (2002) Dynamics of non-isothermal adsorption in packed bed of biporous zeolites. Chemical Engineering Journal, Volume 85, Issues 2–3, Pages 245-257
21. Abd-Elrahman, W.R. Hamed, A.M. El-Emam, S.H. and Awad, M.M. (2011) Experimental investigation on the performance of radial flow desiccant bed using activated alumina. Applied Thermal Engineering, Volume 31, Issues 14–15, Pages 2709-2715
22. Ramzy K. A., Kadoli, R. Ashok Babu, T.P. (2011) Improved utilization of desiccant material in packed bed dehumidifier using composite particles. Renewable Energy, Volume 36, Issue 2, Pages 732-742
23. Hamed, A.M. Abd-Elrahman, W.R. El-Emam, S.H. and Awad, M.M. (2013) Theoretical and experimental investigation on the transient coupled heat and mass transfer in a radial flow desiccant packed bed. Energy Conversion and Management, Volume 65, Pages 262-271
24. Schindler, Bryan J. and LeVan, M. Douglas (2008) The theoretical maximum isosteric heat of adsorption in the Henry's law region for slit-shaped carbon nanopores. Carbon, Volume 46, Issue 4, Pages 644-648
25. Liu, Jian and LeVan, M. Douglas (2009) Isosteric heats of adsorption in the Henry's law region for carbon single wall cylindrical nanopores and spherical nanocavities. Source: Carbon, v 47, n 15, p 3415-3423
26. Yang, Kun., Yao, Ye., Liu, Shiqing. and He, Beixing. (2013) Investigation on applying ultrasonic to the regeneration of a new honeycomb desiccant. International Journal of Thermal Sciences, Volume 72, Pages 159-171
27. Saha, B.B. Akisawa, A. and Kashiwagi, T. (2001) Solar/waste heat driven two – stage adsorption chiller: the prototype. Renew. Energy, pp. 93–101
28. Jiao, A.J. Ma, H.B. and Critser, J.K. (2009) Experimental investigation of cryogenic oscillating heat pipes. International Journal of Heat and Mass Transfer, Volume 52, Issues 15–16, Pages 3504-3509
29. Panyoyai, N. Terdtoon, P. and Sakulchangsatjatai, P. (2009) Effects of aspect ratios and number of meandering turns on performance limit of an inclined closed – loop oscillating heat pipe. International Conference on Science, Technology and Innovation for Sustainable Well-Being (STISWB), 23-24 July 2009, Mahasarakham University, Thailand.
30. Qu, Jian and Wang, Qian (2013) Experimental study on the thermal performance of vertical closed-loop oscillating heat pipes and correlation modeling. Applied Energy, Volume 112, Pages 1154-1160
31. Khandekar, S. Dollinger, N. and Groll, M. (2003) "Understanding operational regimes of closed loop pulsating heat pipes: An experimental study" Appl. Therm. Eng., 23 (2003), pp. 707–719
32. Reay, David, and Kew, Peter. Heat Pipes: Theory, Design and Applications (5th Edition). Jordan Hill, GBR: Butterworth-Heinemann, 2006. ProQuest ebrary. Web. 4 June 2015. Copyright © 2006. Butterworth-Heinemann. All rights reserved.
33. Reay, David, McGlen, Ryan, and Kew, Peter. (2013) Heat Pipes: Theory, Design and Applications (6). Jordon Hill, GB: Butterworth-Heinemann, 2013. ProQuest ebrary. Web. 20 December 2016. Copyright © 2013. Butterworth-Heinemann. All rights reserved.
34. Senjaya, Raffles and Inoue, Takayoshi (2013) Oscillating heat pipe simulation considering bubble generation Part I: Presentation of the model and effects of a bubble generation. International Journal of Heat and Mass Transfer, Volume 60, Pages 816-824

35. Pachgharea, Pramod R. and Mahalleb, Ashish M. (2012) Thermal Performance of Closed Loop Pulsating Heat Pipe Using Pure and Binary Working Fluids. Frontiers in Heat Pipes (FHP), 3, 033002 (2012) DOI: 10.5098/fhp.v3.3.3002
36. Sriudom, Y. Rittidech, S. and Chompookham, T. (2014) The Helical Oscillating Heat Pipe: Flow Pattern Behaviour Study. Advances in Mechanical Engineering. Article ID 194374.
37. Lin, Zirong, Wang, Shuangfeng, Shirakashi, Ryo. and Zhang, L. Winston (2013) Simulation of a miniature oscillating heat pipe in bottom heating mode using CFD with unsteady modeling. International Journal of Heat and Mass Transfer, Volume 57, Issue 2, Pages 642-656
38. Kreith, Frank. Manglik, Raj. M. and Bohn, Mark. S. (2011) Principles of Heat Transfer. 7th Edition. CENGAGE Learning. Pp A12.
39. Karthikeyan, V.K. Ramachandran, K. Pillai, B.C. and Solomon, A. Brusly (2014)Effect of nanofluids on thermal performance of closed loop pulsating heat pipe. Experimental Thermal and Fluid Science, Volume 54, April 2014, Pages 171-178
40. Zhang, Ping. Xuan, YiMin. and Li, Qiang. (2014) A high-precision instrumentation of measuring thermal contact resistance using reversible heat flux. Experimental Thermal and Fluid Science, Volume 54, Pages 204-211
41. Granet, I. and Bluestein, M. (2004) Thermodynamics and Heat Power. 7th Edition. Pearson Prentice Hall. Upper Saddle River, New Jersey. Pp.536-552.
42. Dou, Ruifeng. Ge, Tianran. Liu, Xunliang. and Wen, Zhi. (2016) Effects of contact pressure, interface temperature, and surface roughness on thermal contact conductance between stainless steel surfaces under atmosphere condition. International Journal of Heat and Mass Transfer, Volume 94, March 2016, Pages 156-163
43. Fletcher LS. Recent (1988) Developments in Contact Conductance Heat Transfer. ASME. J. Heat Transfer. 1988;110(4b):1059-1070. doi:10.1115/1.3250610.
44. Xian, Yaoqi. Zhai, Siping . Yuan, Peng. Zhang, Ping. and Yang, Daoguo. (2017) Experimental Characterization Methods for Thermal Contact Resistance: A Review. Applied Thermal Engineering
45. Qu, Jian. Wu, Hui-ying. and Cheng, Ping (2010) Thermal performance of an oscillating heat pipe with Al2O3–water nanofluids. International Communications in Heat and Mass Transfer. Volume 37, Issue 2, Pages 111-115
46. Hao, Tingting. Ma, Xuehu. Lan, Zhong. Li, Nan. Zhao, Yuzhe and Ma, Hongbin. (2014) Effects of hydrophilic surface on heat transfer performance and oscillating motion for an oscillating heat pipe. International Journal of Heat and Mass Transfer, Volume 72, Pages 50-65
47. Zhu, Yue. Cui, Xiaoyu. Han, Hua. and Sun, Shende. (2014) The study on the difference of the start-up and heat-transfer performance of the pulsating heat pipe with water–acetone mixtures. International Journal of Heat and Mass Transfer, Volume 77, Pages 834-842
48. Liu, Xiangdong . Sun, Qing. Zhang, Chengbin and Wu, Liangyu. (2016) High-Speed Visual Analysis of Fluid Flow and Heat Transfer in Oscillating Heat Pipes with Different Diameters. Appl. Sci. 6, 321; doi:10.3390/app6110321
49. Mahapatra, Bishnu N. Das, P.K. and Sahoo, Sudhansu S.(2016) Scaling analysis and experimental investigation of pulsating loop heat pipes. Applied Thermal Engineering, Volume 108, Pages 358-367
50. Khandekar, Sameer. Charoensawan, Piyanun. Groll, Manfred. and Terdtoon. Pradit (2003) Closed loop pulsating heat pipes Part B: visualization and semi-empirical modeling. Applied Thermal Engineering, Volume 23, Issue 16, Pages 2021-2033
51. Khandekar, S. and Groll, M. (2004) An insight into thermo-hydrodynamic coupling in closed loop heat pipes. International Journal of Thermal Sciences, 43 (2004), pp. 13–20
52. Mameli, M. Marengo, M. and Zinna, S. (2012) Numerical model of a multi-turn Closed Loop Pulsating Heat Pipe: Effects of the local pressure losses due to meanderings. International Journal of Heat and Mass Transfer, Volume 55, Issue 4, Pages 1036-1047

53. Schmuller, Joseph. Statistical Analysis with Excel for Dummies, edited by Joseph Schmuller, Wiley, 2013. ProQuest Ebook Central, Created from unnc-ebooks on 2017-02-03 13:53:48.